Journal of Applied Polymer Science

# Effect of the Nanotube Aspect Ratio and Surface Functionalization on the Morphology and Properties of Multiwalled Carbon Nanotube Polyamide-Based Fibers

**Nadka T. Dintcheva,[1] Rossella Arrigo,[2] Giorgio Nasillo,[3] Eugenio Caponetti,[3] Francesco Paolo La Mantia[1]**

[1]Dipartimento di Ingegneria Civile, Ambientale, Aerospaziale, dei Materiali, Università di Palermo, Viale delle Scienze, edificio 6, 90128 Palermo, Italy

[2]Dipartimento di Ingegneria Chimica, Gestionale, Informatica, Meccanica, Università di Palermo, Viale delle Scienze, edificio 6, 90128 Palermo, Italy

[3]Centro Grandi Apparecchiature, Università di Palermo, Via Filippo Marini, 14, 90128 Palermo, Italy

Correspondence to: N. T. Dintcheva (E-mail: nadka.dintcheva@unipa.it)

**ABSTRACT:** In this study, the effect of the carbon nanotube (CNT) aspect ratio and surface functionalization on the mechanical behavior and morphological changes of polyamide (PA)-based fibers was investigated. Composites were prepared by the melt blending of CNTs with PA, and at a later time, the fibers were prepared by melt spinning and cold drawing. A reinforcement effect was noticed for all of the CNTs samples, and the increase in the mechanical properties and dimensional stability was more pronounced for highly oriented filaments. When the elongational flow was increased, the orientation of CNTs along the fiber direction was observed, but the nanotube alignment was much more difficult for CNTs with ultrathin outer diameters because of nanotube waviness and folding. Moreover, the presence of functional groups on the CNT surface hindered their orientation along the fiber direction because some interaction between the functional groups could occur. The morphological variations of the oriented, anisotropic fibers, as studied with transmission electron microscopy, scanning electron microscopy, small-angle X-ray scattering, and differential scanning calorimetry analysis, were correlated with changes in the mechanical behavior. © 2013 Wiley Periodicals, Inc. J. Appl. Polym. Sci. 129: 2479–2489, 2013

**KEYWORDS:** graphene and fullerenes; mechanical properties; morphology; nanotubes; polyamides

Received 7 June 2012; accepted 29 November 2012; published online 30 January 2013

**DOI: 10.1002/app.38898**

## INTRODUCTION

By adding carbon nanotubes (CNTs) into polymeric matrices, one can modify their thermomechanical, mechanical, optical and electrical performances.[1–3] Really, the formulation of CNT-filled polymer-based nanocomposites by melt mixing with good filler dispersion is not easier because of the high polymer viscosity in the melt state and the reaggregation tendency of the nanotubes. A good nanotube dispersion and alignment in the polymeric matrix by melt processing is a very complex phenomenon, and it depends on several factors, including the filler loading, processing apparatus and temperature, screw speed, and residence time, as discussed in the literature.[4–6] Beyond this, the improvement of the mechanical properties of CNT-filled polymers can be achieved with nanotubes with different geometries and aspect ratios. A few studies have suggested that the number of nanotube walls, that is, in single-walled carbon nanotubes (SW-CNTs), double-walled CNTs, or multiwalled carbon nanotubes (MW-CNTs), and the length-to-diameter ratio are very important parameters in the nanotube dispersion and reinforcement of the polymeric matrix.[7–9] Furthermore, in recent years, several studies on the functionalization of the nanofiller surface have been done to improve their compatibility with host matrices[10,11] and water solubility.[12,13] For successful CNT functionalization and/or modification, numerous approaches have been discussed in the literature; they can be summarized as defect functionalization,[14] covalent[15] and noncovalent[16] functionalization, and functionalization through click chemistry.[17]

The formulation of nanofilled polymer-based nanocomposites with good properties and performance by spinning and film blowing is a very important issue.[18] Upon *extensional flow,* that is, the flow involved in spinning and film-blowing processing, the alignment of CNTs along the flow direction is needed in order to improve the composite properties.[19–23] Sennett et al.[19]

showed that MW-CNTs dispersed more quickly into the polycarbonate matrix than SW-CNTs under the same extensional conditions. An interesting study by Bhattacharyya et al.[20] suggested that drawn polypropylene/SW-CNTs fibers are more oriented than unfilled PP fibers. Potschke et al.[21] investigated polycarbonate/MW-CNTs fibers and reported that the curved shape of the MW-CNTs hindered their good alignment and the improvement of their mechanical properties. Moreover, an interesting study by Sandler et al.[22] suggested that the cold drawing did not always induce improvements in the CNT alignment. In particular, the CNT alignment was unfavorable for systems with nanotubes having small outer diameters. In our previous study,[23] we investigated the orientation of both polyamide (PA) macromolecules and CNTs along the extensional flow direction. The formation of a hybrid shish-kebab structure in the MW-CNT/PA nanocomposites was shown. The CNTs played the role of the shish, whereas the PA macromolecules formed the kebab structures; these hybrid shish-kebab structures were responsible for the improvement in the mechanical properties, the dimensional stability, and morphological changes upon extensional flow. In addition, the formation of an MW-CNT bundle and an interesting pull-out phenomenon in the central nanotube upon extensional flow were noticed. Our second study[24] was focused on the effects of different matrices and different nanotube loadings in CNT-filled polymer-based fibers with regard to their final morphology and properties. The obtained results suggest that the PA matrix was the best candidate for the formulation of CNT-filled fibers with respect to the other investigated systems, that is, polyethylene and polystyrene.

In this study, the effect of both the aspect ratio and nanotube functionalization on the morphology and properties of CNT PA-based fibers were studied. CNTs having different aspect ratios and different functional groups (—OH and —COOH) on their surface were used for fiber formulation. All of the CNT samples we used exerted reinforcement effects, and this effect was more pronounced for the CNTs having the largest outer diameter (lowest aspect ratio) and without functional groups. Moreover, the orientation of the CNTs having an ultrathin outer diameter (and the highest aspect ratio) was much more difficult than the orientation of the CNTs with a large outer diameter because of the nanotubes' intrinsic waviness and their folding tendency, which hindered the alignment. Additionally, the presence of both functional groups, that is, —OH and —COOH groups, on the CNT surface made filament formation difficult and hampered the nanoparticle alignment along the extensional flow direction because of interaction within the polymeric chains.

## EXPERIMENTAL

### Materials

The materials used in this study were (1) PA 6 commercialized by the Radici Group (Bergamo, Italy) under the name of Radilon S (density = 1.13 g/cm$^3$ and intrinsic viscosity = 1.5 dL/g measured at 30°C in 80 vol % formic acid) and (2) MW-CNTs having different aspect ratios and surface functionalizations. In Table I, their main characteristics are reported. The CNTs were added at 3% w/w on the basis of our previous experimental investigations and results.[23,24]

### Processing

The preparation of the PA/CNTs system was carried out with a Brabender (Duisburg, Germany) mixer at a temperature ($T$) of 240°C and a mixing speed of 50 rpm for 5 min. The nanotubes were added to the melted PA after 2 min. The pristine PA was subjected to the same processing.

The fibers were spun with a capillary viscometer (Rheoscope 1000, CEAST, Torino, Italy) operating under a constant extrusion speed (5 mm/min), with a die of 1 mm diameter ($D_o$) at 240°C. The filaments were extruded in air at room temperature. The take-up velocity was about 4 m/min. The final diameter of the as-spun fibers ($D_f$) was about 0.3 mm, and the draw ratio (DR) was about 10.

The spun fibers were drawn with the aid of an Instron (Milano, Italy) machine (model 3365) at room temperature and at a crosshead speed of 100 mm/min. The initial length was 30 mm in all cases. The amount of drawing was characterized by the DR:

$$\mathrm{DR} = L_f / L_o$$

where $L_f$ is the final length and $L_o$ is the initial length of the fiber.

### Characterization

**Rheological Characterization.** The rheological characterization, including the measurement of the complex viscosity ($\eta^*$) and storage and loss moduli ($G'$ and $G''$), was performed with a Rheometric Scientific RDA II plate–plate rotational rheometer operating at $T = 240$°C.

The rheological behavior in nonisothermal elongational flow was tested with the previously described capillary viscometer equipped with a drawing system. The capillary diameter was 1 mm, the length-to-diameter ratio was 40, and the test temperature was 240°C. The extruded filament was driven through a pulley system and was then drawn with two counterrotating rolls. We carried out the run was by pulling the filament, extruded at a given flow rate, at a rotational speed that increased with a linear acceleration of 100 rpm/s. The test ended with the filament breaking. The force at break of the molten filament was read directly and is known as the *melt strength* (MS). The breaking stretching ratio (BSR) was calculated as the ratio between the drawing speed at break and the extrusion speed at the die.

**Mechanical Characterization.** Mechanical tests of the fibers were carried out with an Instron universal testing machine (model 3365) according to ASTM D 882. The elastic modulus ($E$) was measured at a speed of 1 mm/min. When the deformation was about 10%, the crosshead speed was increased to 100 mm/min until break. The values for $E$, tensile strength (TS), and elongation at break (EB) were calculated as the average of 10 tests. The standard deviations are reported in the figures.

**Thermal Analysis.** The calorimetric data were evaluated by differential scanning calorimetry (DSC) with a PerkinElmer (Waltham, MA, USA) DSC7 at scanning rate of 10°C/min.

**Morphological Analysis.** Scanning electron microscopy (SEM) investigation was performed on the nitrogen-fractured radial surfaces of all of the fibers by a Philips ESEM XL30 instrument (Amsterdam, Netherlands).

**Table I.** Description, Code, and Main Characteristics of All of the CNTs

| Description | Code | Supplied by | Main characteristics |
|---|---|---|---|
| MW-CNTs with a large outer diameter | CNTs(l) | Sigma-Aldrich (St. Louis, MO, USA) | Outer diameter > 150 nm |
| | | | Length = 5–10 μm |
| | | | Carbon content > 90% |
| | | | Density = 2.1 g/mL at 25°C obtained through chemical vapor deposition |
| MW-CNTs with a thin outer diameter | CNTs(th) | Cheap Tubes (Brattleboro, VT, USA) | Outer diameter > 50 nm |
| | | | Length = 10–20 μm |
| | | | Purity > 95 wt % |
| | | | Ash < 1.5 wt % obtained through catalytic chemical vapor deposition |
| —OH functionalized MW-CNTs with a thin outer diameter | CNTs(th)—OH | Cheap Tubes | Outer diameter > 50 nm |
| | | | Length = 10–20 μm |
| | | | Purity > 95 wt % |
| | | | Ash < 1.5 wt % |
| | | | —OH content = 0.5–1.0 wt % |
| —COOH functionalized MW-CNTs with a thin outer diameter | CNTs(th)—COOH | Cheap Tubes | Outer diameter: > 50 nm |
| | | | Length = 10–20 μm |
| | | | Purity > 95 wt % |
| | | | Ash < 1.5 wt % |
| | | | —COOH content = 0.5–1.0 wt % |
| MW-CNTs with an ultrathin outer diameter | CNTs(uth) | Politecnico di Milano (Milano, Italy) | Outer diameter < 20 nm |
| | | | Length = 20–30 μm |
| | | | Purity < 90% obtained through catalytic chemical vapor deposition |

Transmission electron microscopy (TEM) observations were performed at the Centro Grandi Apparecchiature–UninetLab, University of Palermo. The analyses were carried out on the isolated nanotubes and on the radial surfaces of the fibers. Ultrathin films with a thickness of about 100 nm for TEM observation were prepared via cutting from the epoxy block with a Leica (Solms, Germany) Ultramicrotome EM-UC6. Ultrathin slides of the fibers at different DRs were mounted on the lacey carbon films on 300-mesh copper grids and were then observed by a JEOL (Tokyo, Japan) JEM-2100 instrument under an accelerated voltage of 200 kV.

Small-angle X-ray scattering (SAXS) measurements were made with Bruker (Billerica, MA, USA) AXS Nanostar-U instrument with Cu Kα radiation emitted by a rotating anode source set to 40 kV and 18 mA. X-rays were made parallel with a couple of Göbel mirrors and were collimated with a series of three pinholes with diameters of 500, 150, and 500 $\mu$m. The samples were directly mounted on the sample stage to prevent additional scattering of the holder.

The data, collected at room temperature, were recorded with a two-dimensional multiwire proportional counterdetector placed 26 cm from the sample; we obtained a momentum transfer ($Q$) range between 0.02 and 0.75 $\text{Å}^{-1}$:

$$Q = 4\pi \sin \theta/\lambda$$

where $2\theta$ is the scattering angle.

## RESULTS AND DISCUSSION

### Effect of the Nanotube Aspect Ratio

**Rheological Characterization.** In Figure 1(a,b), $\eta^*$, $G'$, and $G''$ as functions of the frequency of the unfilled PA and CNT (having different aspect ratios)-filled PA are reported. In the

Applied Polymer SCIENCE

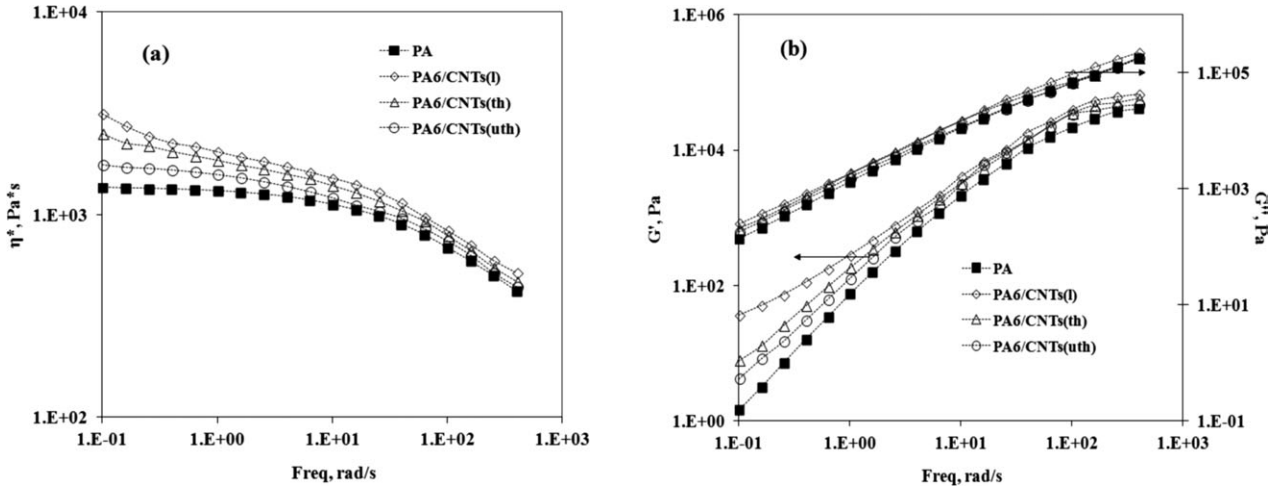


**Figure 1.** (a) $\eta^*$ and (b) $G'$ and $G''$ as a function of the frequency of the unfilled and CNT-filled PA.

low-frequency region, the nanotube loading significantly influenced the viscosity of PA; in particular, the viscosity values depended on the nanotube dimensions, see Figure 1(a). The addition of the CNTs with the largest outer diameter (and the lowest aspect ratio) led to the highest viscosity increase, whereas the addition of the CNTs with thin and ultrathin outer diameters led to less pronounced viscosity increases. The CNTs(l) caused the disappearance of the Newtonian behavior shown by neat PA in the low-frequency region, and they were also responsible for the more pronounced shear-thinning behavior in the high-frequency region. The presence of the CNTs(th) and CNTs(uth) led to an increase in the viscosity values but did not substantially modify the rheological behavior of PA in the investigated frequency range.

The trend of $G'$ and $G''$ reflected the observed trend of the flow curves [see Figure 1(b)]. Indeed, the $G'$ curves of the nanocomposites were strongly higher than that of the unfilled PA matrix, and in particular, the CNT(l)-filled PA sample showed the highest $G'$ values. At very low frequencies, the $G'$ curve of this system showed a small slope; rather, the curve tended to become flat. This behavior, together with the increase in the viscosity values at very low frequency showed before, suggested a solidlike behavior for the CNT(l)-filled PA nanocomposite, typical for structured melt. This feature did not seem to be present for the other two systems, at least in the investigated frequency range. The solidlike behavior shown by the CNT(l)-filled PA nanocomposite was due to the ability of the CNTs(l) to interact between them and form a semi-three-dimensional (semi-3D) structure. The CNTs(th) and CNTs(uth), because of their intrinsic waviness and folding tendency, reduced their effective length and, thus, decreased the interaction between the nanotubes. So, these kinds of nanotubes were not able to form the semi-3D structure.

To evaluate the effect of the nanotube aspect ratio on the rheological behavior in nonisothermal elongational flow, the MS and BSR values of all of the investigated samples were measured. The investigation into the nonisothermal elongation flow gave useful information about the nanocomposite ability in processing operations, such as spinning and film blowing, where this type of flow was involved. The measured MS and BSR values at a 60-$s^{-1}$ apparent shear rate of the unfilled and CNT-filled PA samples are reported in Table II(a). The MS was significantly influenced by the presence of CNTs; the addition of CNTs(l) led to a rise in the MS value of about 80% with respect to the value of the unfilled PA, whereas CNT(th) and CNT(uth) loading increased the MS value of about 70 and 55%, respectively. Usually, a microfiller presence involves an increase in MS together with a decrease in the BSR value.[25] In this study, a small reduction in the BSR values with CNT addition confirmed the possibility of processing all of the investigated systems in spinning and film-blowing processing.

Many articles have been published on the effect of fillers on the rheological behavior of polymer matrices and, in particular, on the effect of the geometry of inert, undeformable particles. All of the experimental data agree that the lower the diameter of the particles is, the higher the increase of the matrix viscosity will be and that the higher the aspect ratio of the fillers is, the higher the increase in the viscosity will be. This behavior has been interpreted considering a decrease in the particle size and an increase in the aspect ratio, the interfacial area between

**Table II.** MS and BSR of the (a) Unfilled and CNT-Filled PA and (b) CNT(th)—OH- and CNT(th)—COOH-Filled PA at an Apparent Shear Rate of 60 $s^{-1}$

| Sample | MS (cN) | BSR |
|---|---|---|
| (a) | | |
| PA | 2.3 | 47 |
| PA + CNTs(l) | 4.2 | 39 |
| PA + CNTs(th) | 3.9 | 38 |
| PA + CNTs(uth) | 3.6 | 35 |
| (b) | | |
| PA + CNTs(th)—OH | 3.7 | 35 |
| PA + CNTs(th)—COOH | 3.7 | 36 |

**Table III.** Mechanical Properties of the (a) Unfilled and CNT-Filled PA and (b) CNTs(th)—OH and CNTs(th)—COOH-Filled PA Fibers at the Lowest DR (DR = 1)

| Sample | *E* (MPa) | TS (MPa) | EB (%) |
|---|---|---|---|
| (a) | | | |
| PA | 1050 ± 52 | 110 ± 5.5 | 764 ± 38 |
| PA + CNTs(l) | 1230 ± 61 | 102 ± 5.1 | 540 ± 27 |
| PA + CNTs(th) | 1255 ± 62 | 105 ± 5.2 | 550 ± 27 |
| PA + CNTs(uth) | 1092 ± 50 | 75 ± 3.7 | 318 ± 15 |
| (b) | | | |
| PA + CNTs(th)—OH | 1322 ± 66 | 98 ± 4.9 | 355 ± 17 |
| PA + CNTs(th)—COOH | 1365 ± 68 | 95 ± 4.7 | 283 ± 14 |

matrix and particles will increased, so the stress between the two phases can be better transmitted. Moreover, the increase in the particle aspect ratio prevents the flow of the macromolecules. The reported data showed the opposite behavior because the increase in the viscosity was higher with decreasing aspect ratio. We hypothesized that the rheological behavior of this nanocomposite could not be predicted with the initial aspect ratio of the nanotubes because the thinner nanotubes could be easily deformed during the flow, and this would change their aspect ratio. In the following text, this hypothesis is demonstrated for the fibers.

### Mechanical Characterization

In Table III(a) and Figures 2 and 3, the main mechanical properties, that is, *E*, TS, and EB for the unfilled PA and all of the CNT-filled PA fibers, both as-spun and drawn, are reported. For the drawn fibers, the data are reported in dimensionless form (the value of the drawn fiber divided by that of the as-spun fiber) as a function of the DR. The presence of all of the CNT types in the as-spun fibers led to an increase in *E* and a decrease in the properties at break [see Table III(a)]. In particular, the CNT(uth) loading induced a significant decrease in both TS and EB, whereas *E* was almost unchanged with respect to

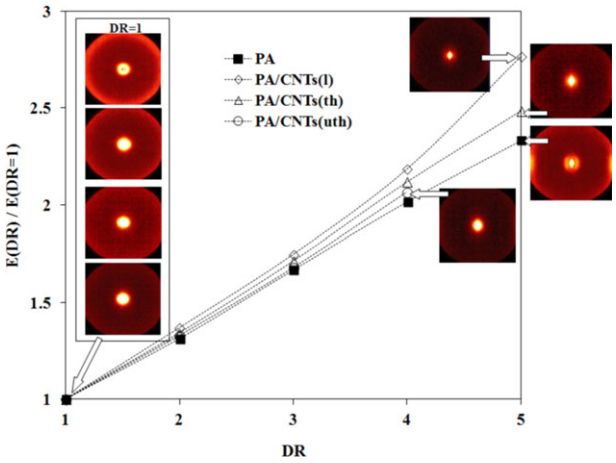


**Figure 2.** Dimensionless *E* as a function of the DR and SAXS patterns at DR = 1 and the maximum of the unfilled and CNT-filled PA fibers. [Color figure can be viewed in the online issue, which is available at wileyonlinelibrary.com.]

the unfilled PA fibers. On the contrary, the two systems with CNTs(l) and CNTs(th) showed similar results; in particular, the modulus increased by about 20%, and with increasing cold DR, *E* and TS increased for all of the investigated fibers, whereas EB decreased.[21,23] The reinforcement effect due to the CNT presence, especially at high cold DRs (DRs = 4 and 5) was more pronounced for the CNTs with the lowest aspect ratio. The CNTs with thin and ultrathin outer diameters exert a reduced reinforcement for the PA fibers. It was interesting to highlight that the maximum applied drawing for the CNT(uth)-filled PA fibers was DR = 4; this indicated some difficulty in filament formation.

To compare the theoretical *E* values and the experimental data, several predictive models for two-component composite materials[26,27] were used. In this article, we compare the experimental data with that obtained, considering the three most used models (see later discussion).

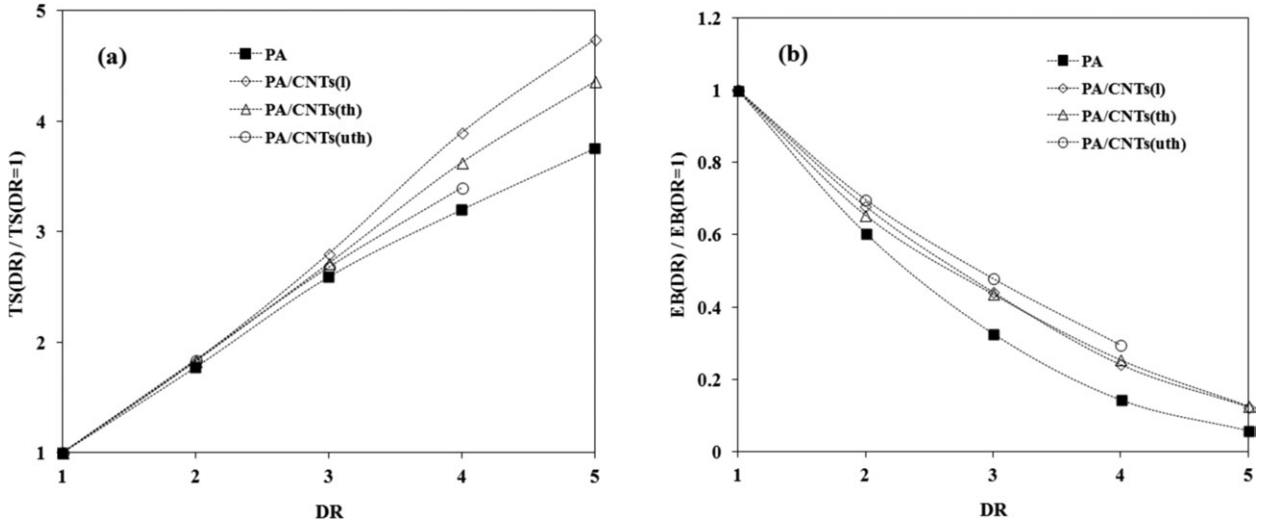


**Figure 3.** (a) Dimensionless TS and (b) EB as a function of the DR of the unfilled and CNT-filled PA fibers.

Applied Polymer SCIENCE

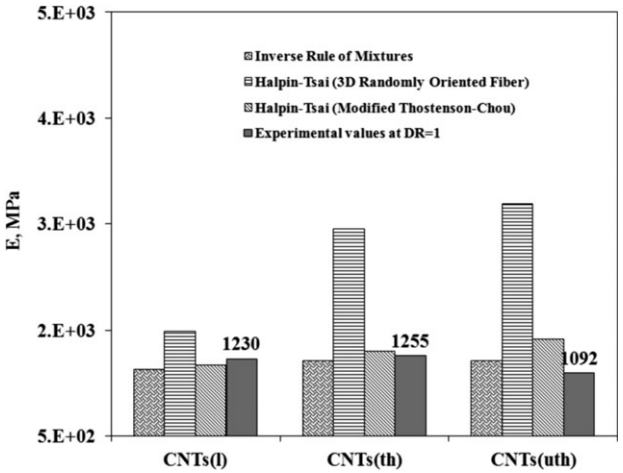


**Figure 4.** Theoretical models for the prediction of *E*.

The predicted values of *E* according to the previous models were compared with the experimental data at DR = 1 (see Figure 4). Really, the inverse rule of mixtures model does not consider the filler aspect ratio, but the estimated values were near the experimentally obtained values. The theoretical calculated values, determined with the Halpin–Tsai rule (3D), overestimated the experimental values, even more for CNTs(uth). This kind of CNT can be deformed during the flow, as discussed previously.

The theoretical models and equations are as follows:

$$\text{Inverse rule of mixtures (parallel model)}: \quad \frac{1}{E_c} = \frac{V_m}{E_m} + \frac{V_f}{E_f}$$

$$\text{Halpin}-\text{Tsai27 (3D randomly oriented fibers)}: \quad E_c = \frac{1}{5}E_L + \frac{4}{5}E_T$$

$$\frac{E_L}{E_m} = \frac{1 + 2(L/d)\eta_L V_f}{1 - \eta_L V_f}$$

$$\frac{E_T}{E_m} = \frac{1 + 2\eta_T V_f}{1 - \eta_T V_f}$$

$$\eta_L = \frac{(E_f/E_m) - 1}{(E_f/E_m) + 2(L/d)}$$

$$\eta_T = \frac{(E_f/E_m) - 1}{(E_f/E_m) + 2}$$

For the Halpin–Tsai (modified Thostenson–Chou) method,[28] the only difference was that, here, the MW-CNTs modulus was evaluated as follows:

$$E_{\text{eff}}(\text{effective modulus of CNTs}) = \frac{4t}{d}E_{NT}$$

where $E_{NT}$ (theoretical modulus of carbon nanotube) = 1 TPa ($t$ = 0.34 nm) and is the distance between the nanotube walls, $E_c$ is the composite tensile modulus, $V_f$ is the volume fraction of the filler, $V_m$ is the volume fraction of the matrix, $E_f$ is the tensile modulus of the filler (ca. 1 TPa), $E_m$ is the tensile modulus of the matrix, $E_L$ is the longitudinal composite tensile modulus, $E_T$ is the transverse composite tensile modulus, $L$ is the filler length, and $d$ is the filler diameter.

Also, their effective aspect ratio was not constant (due to the intrinsic waviness), and it was different than the value used for the calculations. Furthermore, the theoretical calculated values, determined with the Halpin–Tsai one-dimensional and two-dimensional (not reported) rules, appeared to be excessively overestimated than the experimental values; this indicated that for reinforcement elements, no preferential orientation could be identified. In fact, the Halpin–Tsai rule (3D) gave values closer the experimental values; this suggested some random 3D orientation of the reinforcement elements. The differences between the experimental values and the values calculated with the Halpin–Tsai rule (3D) probably could be attributed to the variation in the initial aspect ratio of the nanotubes because of their folding and intrinsic waviness. In fact, the discrepancies were more pronounced for the CNTs(th) and even more so for the CNTs(uth). The Halpin–Tsai rule, the modified Thostenson–Chou model, was able to predict the experimental values for the CNTs(l) and CNTs(th), whereas this model overestimated the value for the CNTs(uth) because of the reasons listed previously.

To evaluate the dimensional stability of the filament, the shrinkage values as a function of DR were measured (see Figure 5). The unfilled PA filaments showed a minor dimensional stability compared to all of the nanocomposites filaments, so the nanotube presence made the nanocomposite fibers more dimensionally stable. All of the trends showed a maximum, which could be explained by some structural changes in the PA morphology (e.g., orientation of the macromolecules upon extensional flow); the nanotube presence made this issue less marked. Once again, the CNT(l) loading led to better performance in comparison with the other nanotube kinds.

**DSC.** In Figure 6, the DSC trace of the first heating and cooling of all of the as-spun fibers of the unfilled and CNT-filled PA are plotted, and in Table IV(a), the main thermal properties of the as-spun and drawn fibers are reported. The as-spun PA filament showed a small shoulder at about 210°C because of the presence

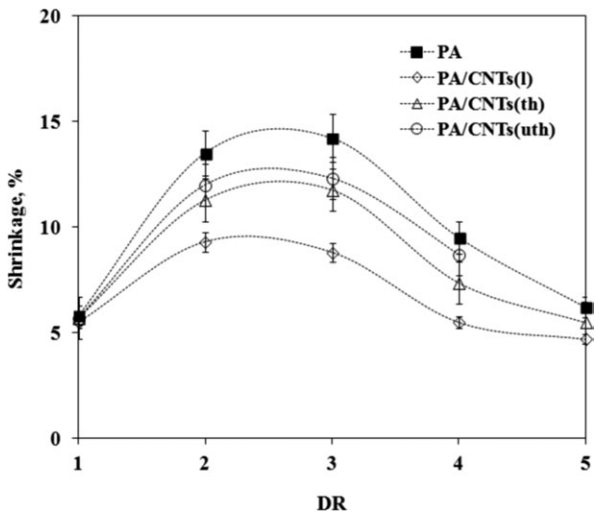


**Figure 5.** Shrinkage as a function of the DR of the unfilled and CNT-filled PA fibers after thermal treatment at 120°C for 10 min.

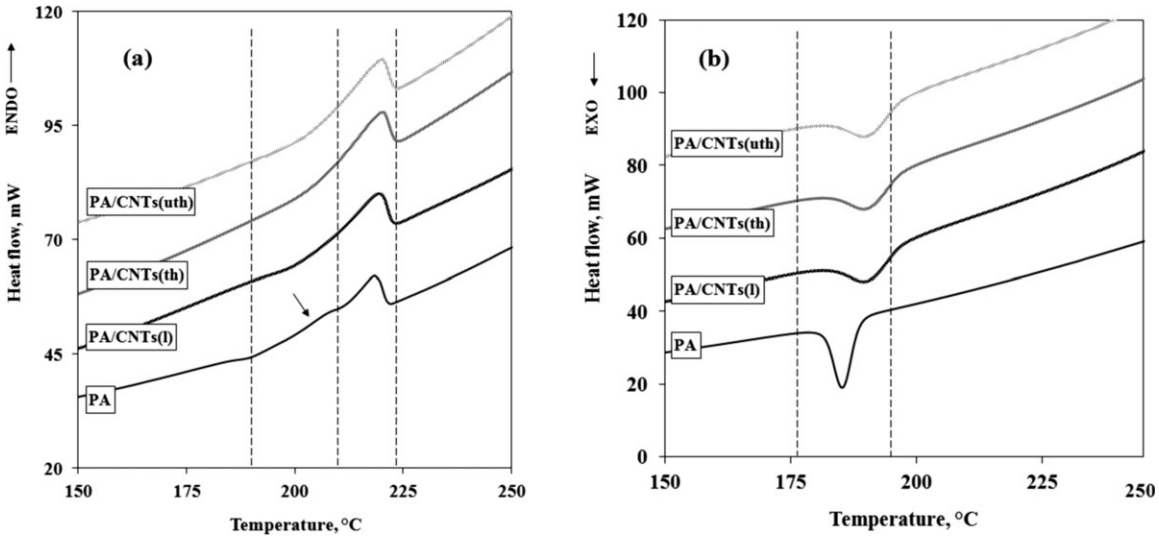


**Figure 6.** DCS traces of the (a) first heating and (b) cooling of the unfilled and CNT-filled PA fibers at the lowest DR (DR = 1).

of a small amount of γ-crystalline form; this crystalline form disappeared after cold drawing. The disappearance of the γ-crystalline form in the PA could be observed upon CNTs loading [see Figure 6(a)]; this was in agreement with our previous investigation.[23] Really, all of the drawn unfilled and filled fibers showed a very distinct melting peak at about 218°C because of the PA α-crystalline form. The CNT loading led to a decrease in the melting enthalpy, and the reduction was about 8% for the sample with the CNTs(l) and about 3% for the sample filled with the CNTs(uth). These decreased were smaller at the maximum DR. Very similar considerations could be made about the crystallization behavior of the nanocomposites systems with respect to the unfilled matrix [see Figure 6(b) and Table IV(a)]. In particular, the increase in the crystallization temperature and the reduction of the crystallization enthalpy by CNT addition suggested that the nanofiller presence destroyed the matrix crystallinity, and no nucleation effect occurred.

**Morphological Characterization.** The morphology of the unfilled and CNT-filled PA fibers were investigated by SAXS, TEM, and SEM analysis. The two-dimensional SAXS patterns of the as-spun and drawn-at-maximum DR fibers are shown in Figure 2. The unfilled PA and all of the CNT-filled PA as-spun fibers showed isotropic scattering and were very similar. At the maximum DR, the anisotropy of the patterns increased because of the morphological changes in the structure of PA. It seemed that the anisotropy of the CNT(l)-loaded PA-based fibers was higher than that of the CNT(uth)-PA-based fibers.

Obviously, the higher anisotropy for the CNT(l)–PA systems could be explained by the ability of the nanofiller with the smaller aspect ratio in the orientation along the fiber direction after the drawing. Conversely, the CNTs(uth) showed some difficulty in orientation along the fiber direction because of their folding, intrinsic waviness, and ultrathin diameter. So, the CNT(uth)/PA fibers showed a smaller anisotropy with respect to the other investigated systems.

In addition, TEM and SEM analyses were performed to examine the distribution of the CNTs with different aspect ratios into the PA matrix before and after drawing [see Figure 7]. The observations suggested that the orientation of all of the CNTs samples upon extensional flow occurred, but this orientation

**Table IV.** Melting Temperature ($T_m$), Melting Enthalpy ($\Delta H_m$), Crystallization Temperature ($T_c$), and Crystallization Enthalpy ($\Delta H_c$) of the First Scans for the (a) Unfilled and CNT-Filled PA and (b) CNTs(th)—OH and CNTs(th)—COOH-Filled PA Fibers at the Lowest and Highest DRs

| | DR = 1 | | | | Maximum DR | | | |
|---|---|---|---|---|---|---|---|---|
| Sample | $T_m$ (°C) | $\Delta H_m$ (J/g) | $T_c$ (°C) | $\Delta H_c$ (J/g) | $T_m$ (°C) | $\Delta H_m$ (J/g) | $T_c$ (°C) | $\Delta H_c$ (J/g) |
| (a) | | | | | | | | |
| PA | 218.2, 209.5[a] | 60.5 | 185.1 | 54.8 | 219.0 | 64.8 | 184.6 | 55.7 |
| PA + CNTs(l) | 218.8 | 56.4 | 189.9 | 44.6 | 218.5 | 63.1 | 188.9 | 47.0 |
| PA + CNTs(th) | 219.2 | 57.1 | 189.0 | 44.1 | 219.1 | 62.5 | 188.2 | 46.5 |
| PA + CNTs(uth) | 218.9 | 58.5 | 189.0 | 43.8 | 219.0 | 63.4 | 187.8 | 46.7 |
| (b) | | | | | | | | |
| PA + CNTs(th)—OH | 219.0 | 58.2 | 188.5 | 44.0 | 218.4 | 63.1 | 188.0 | 46.1 |
| PA + CNTs(th)—COOH | 219.8 | 58.0 | 188.7 | 43.9 | 219.0 | 62.1 | 188.2 | 46.3 |

[a]Small shoulder at this point.

Applied Polymer SCIENCE

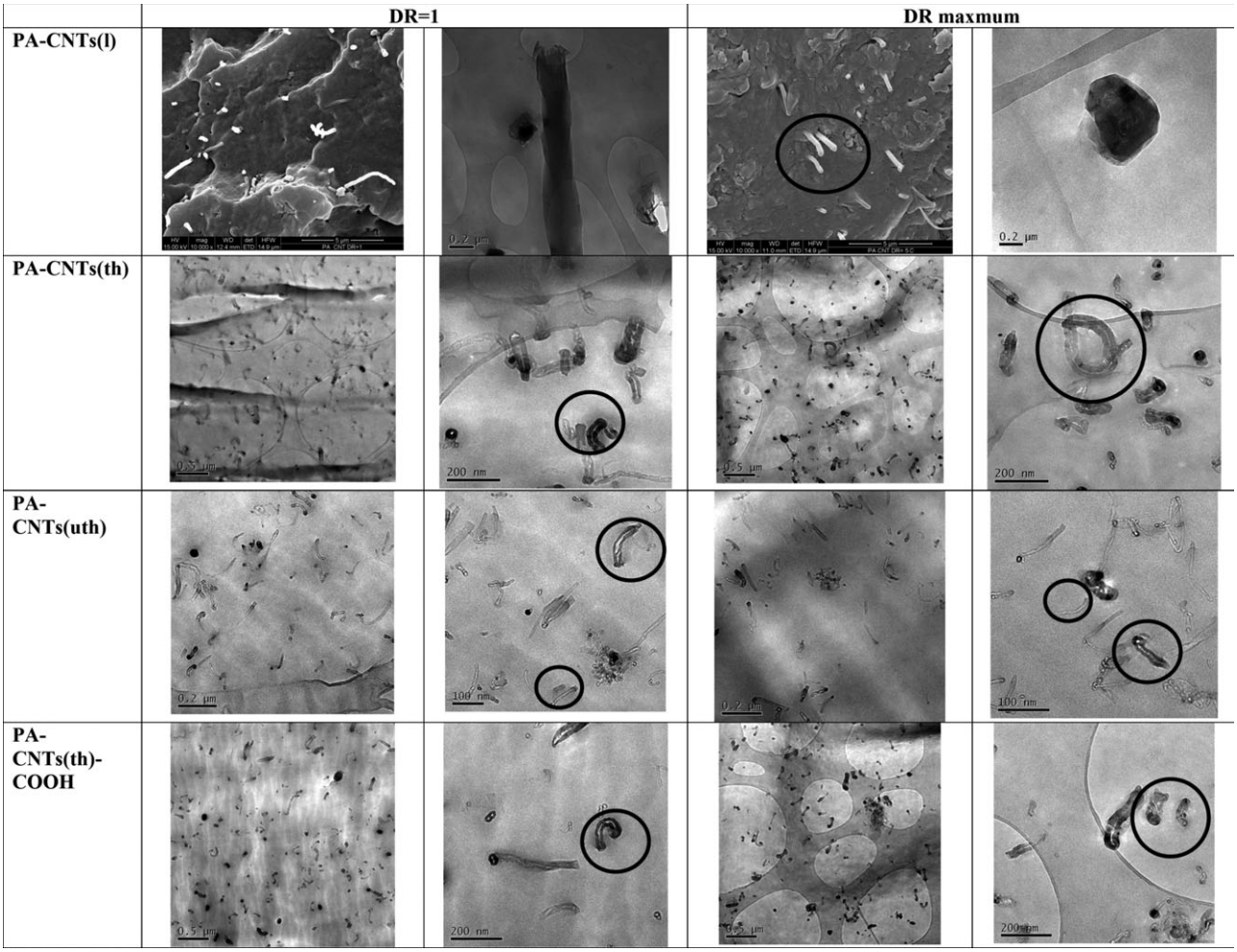


**Figure 7.** TEM and SEM micrographs of the PA-based fibers loaded with CNTs having different aspect ratios and CNTs(th)—COOH at the lowest and highest DRs at different magnifications.

was much easier for the CNTs(l) with the lowest aspect ratio; this was in agreement with our previous investigation[23,24] and with the SAXS analysis. The CNT(th)- and CNT(uth)-PA-based fibers, both as-spun and drawn, showed waviness and folding; this hindered the nanotube orientation upon extensional flow. Finally, the best reinforcement effect, exercised by the CNTs(l)

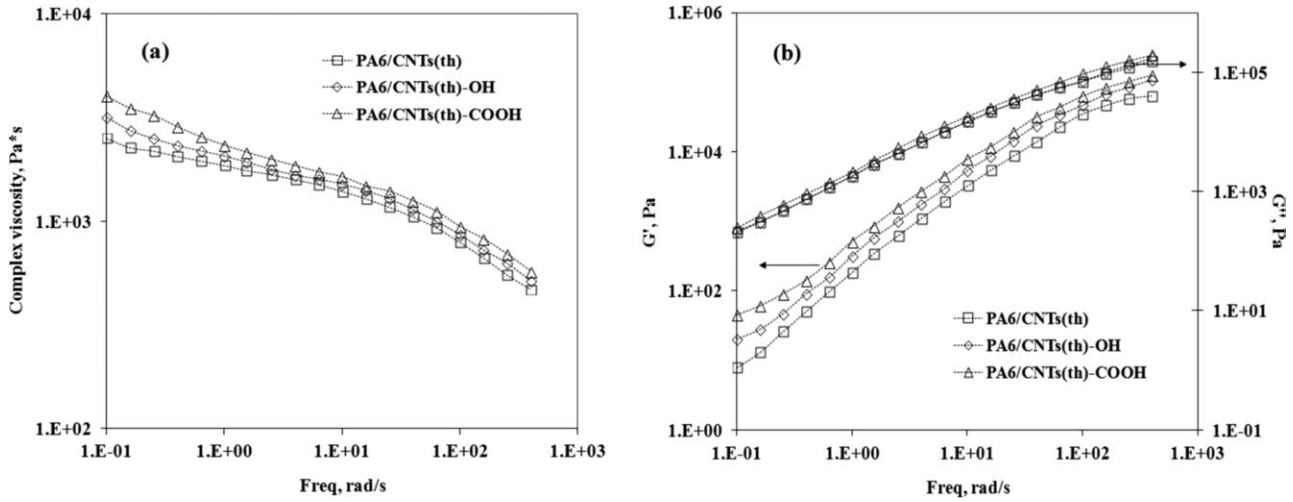


**Figure 8.** (a) $\eta^*$ and (b) $G'$ and $G''$ as a function of the frequency of CNTs(th) and functionalized CNT(th)-filled PA.

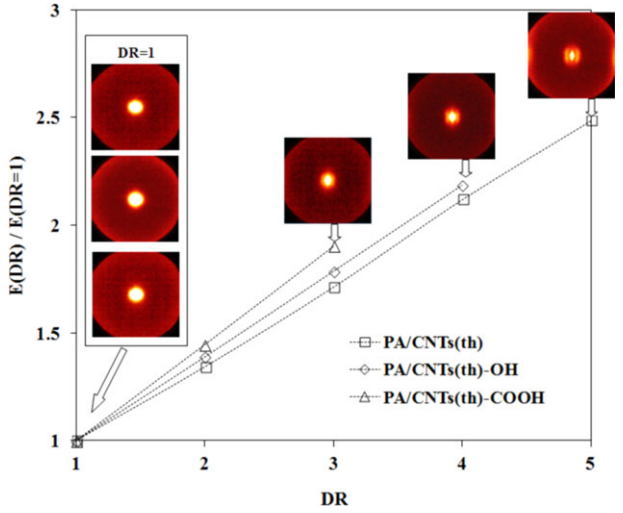


**Figure 9.** Dimensionless *E* as a function of the DR and SAXS patterns at DR = 1 and maximum of CNTs(th) and functionalized CNT(th)-filled PA fibers. [Color figure can be viewed in the online issue, which is available at wileyonlinelibrary.com.]

with the lowest aspect ratio and observed by mechanical testing, could be explained by the results of the morphological analysis: this kind of nanotube was able to be aligned upon extensional flow, and this issue was responsible for the improved *E* and dimensional stability values so the fibers.

### Effect of the Surface Functionalization

**Rheological Characterization.** $\eta^*$, $G'$, and $G''$ as functions of the frequency of the CNT(th)-and functionalized CNT(th)-PA-based samples were measured [see Figure 8(a,b)]. The presence of the functional groups on the CNT outer surface increased the interaction in the molten state between the nanotubes and the PA macromolecules, and this was confirmed by the rise of $\eta^*$. Indeed, the viscosity curves of the nanocomposites with functionalized nanotubes were higher than that of the PA/CNT(th) sample in the investigated frequency region and showed a very distinct yield stress behavior typical of structured systems; this suggested some interaction between the nanotubes and macromolecular functional groups.

**Mechanical Characterization.** The main mechanical properties of the as-spun fibers are reported in Table II(b), and in Figures 9 and 10, the dimensionless *E,* TS, and EB for the drawn fibers as a function of the DR are plotted. The modulus of the as-spun fibers increased in the presence of the functionalized nanotubes, whereas the properties at break (TS and EB) decreased. This meant that the maximum DR achievable by these samples was slower than that obtained for the nanocomposite with the same unfunctionalized nanotubes. The increase in the modulus and the decrease in EB should be interpreted as a better orientation of the macromolecules and the nanotubes along the drawing direction. The lower values of TS was probably due to the premature rupture of the samples. This better orientation could arise from the better adhesion between the macromolecules and nanotubes, which allowed a better transmission of the stress from the polymer to the filler. The *E* versus DR curves of the nanocomposites with the functionalized nanotubes increased more rapidly than that of the nanocomposites with the unfunctionalized nanotubes, but because of the lower DR achievable, the maximum modulus obtained was lower than that measured for the CNT(th)/PA fibers. The lower EB of these fibers suggested, together with the other results, a better orientation for these fibers.

The better dimensional stability of the nanocomposites with the nanotubes previously observed was confirmed by the data relative to the fibers with the functionalized nanotubes [see Figure 11]. The functional groups on the CNT(th) surface made the PA filaments more stable in dimensional terms; that is, the shrinkage values were lower than the values of the PA/CNT(th) filaments at different DRs. The interactions between the functional groups coming from the matrix and the functionalized CNT(th) surface increased the rigidity and dimensional stability of the nanocomposites, but subsequently, the ductility of the systems was penalized.

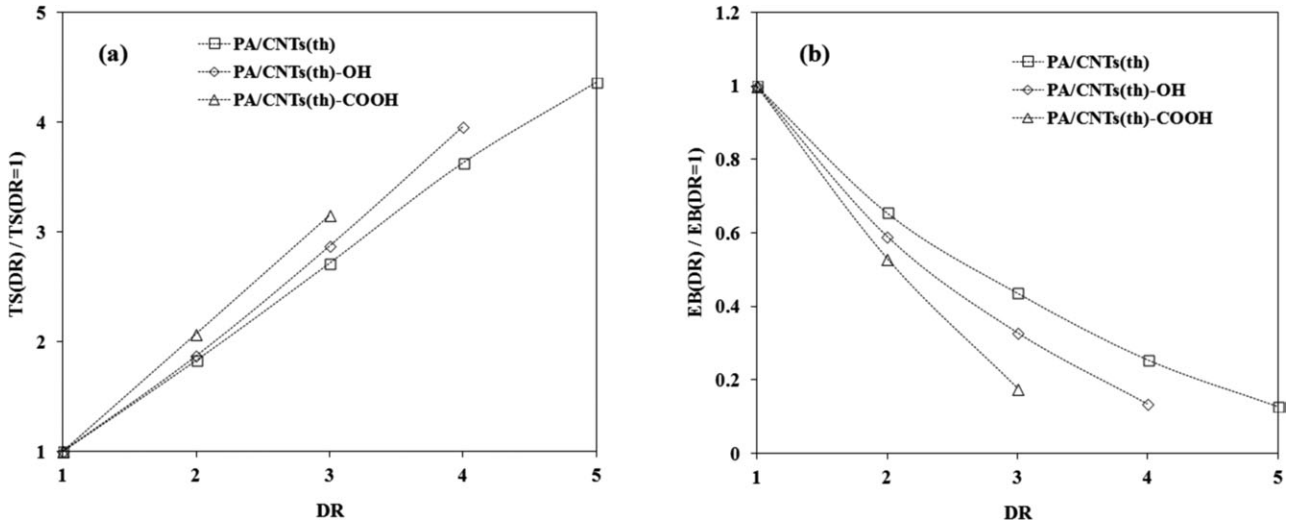


**Figure 10.** (a) Dimensionless TS and (b) EB as a function of the DR of CNTs(th) and functionalized CNT(th)-filled PA fibers.

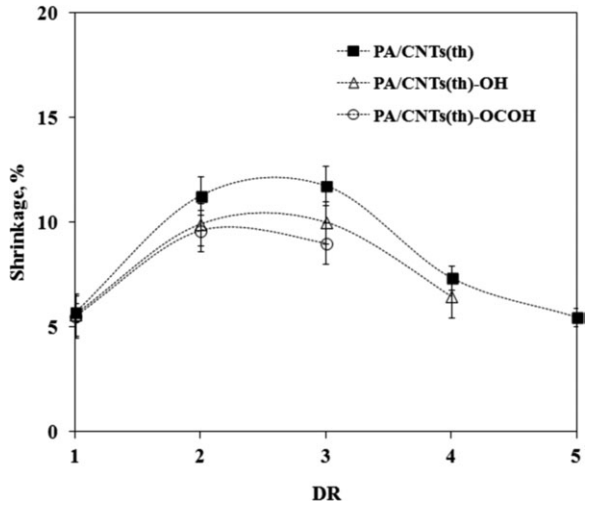


**Figure 11.** Shrinkage as a function of the DR of CNTs(th) and functionalized CNT(th)-filled PA fibers after thermal treatment at 120°C for 10 min.

**DSC.** In Figure 12, the DSC traces of the first heating and cooling of PA/CNTs(th) without and with functional groups are plotted, and in Table IV(b), the main thermal properties before and after drawing are reported. It seemed that the —OH and —COOH groups on the CNT(th) surface did not modify the crystallinity of PA. Moreover, the DSC traces showed melting peaks only at about 219°C due to the PA crystalline $\alpha$ form. The crystalline $\gamma$ form disappeared (with no shoulder at about 210°C) with the loading of CNTs(th) and functionalized CNTs(th) both before and after drawing. The cooling behavior of the PA/CNTs(th) and the PA/functionalized CNTs(th) were very similar [see Figure 12(b) and Table IV(b)]; this suggested no influence of the interaction between the functional groups on the polymeric matrix crystallization.

**Morphological Characterization.** The two-dimensional SAXS patterns before and after the drawing of the CNTs(th) without and with functional group PA-based filaments are reported in Figure 9. At DR = 1, the three investigated systems showed very similar isotropic scatterings. Furthermore, at the maximum DR [which was different for the PA/CNTs(th), PA/CNTs(th)—OH, and PA/CNTs(th)—COOH; i.e., DR = 5, 4, and 3, respectively], the anisotropy of the patterns increased.

In addition, the TEM micrographs suggested that the dispersion and distribution of the CNTs(th) and CNTs(th)—COOH into PA at DR = 1 and at the maximum DR were very similar, although the —COOH functionalized CNTs(th) showed a tendency toward reaggregation [see Figure 7]. The interaction between the functional groups and the observed waviness and folding could be invoked to explain the reduced ability in the drawing of the PA/CNTs(th)—COOH system.

## CONCLUSIONS

CNTs having different aspect ratios and different surface functionalizations were considered for PA-based melt-spinning fiber formulation. After the fiber formulation, all of the filaments were subjected to cold extensional flow. All of the CNTs exerted reinforcement effects on the PA matrix, and, moreover, the improvement of the mechanical properties and the increase of the dimensional stability were more pronounced for highly oriented filaments. The achieved mechanical improvements and dimensional stability of the PA-based filaments followed the sequence CNTs(l) > CNTs(th) > CNTs(uth). Moreover, the CNTs(l) having lowest aspect ratio showed a great ability for orientation along the flow direction, whereas the CNTs(th) and CNTs(uth) showed waviness and folding in both conditions before and after drawing. Additionally, the presence of functional groups on the CNT surface hindered the nanotube orientation along the fiber direction because of the interaction between the functional groups in the macromolecules and those on the nanotube surface. The increase in $E$ achieved at DR = 5, 4, and 3 for CNTs(th), CNTs(th)—OH, and CNTs(th)—COOH, respectively, was similar; this indicated a reduced ability of the functionalized CNTs in filament formation. The TEM analysis showed CNT waviness and folding in both the lowest and

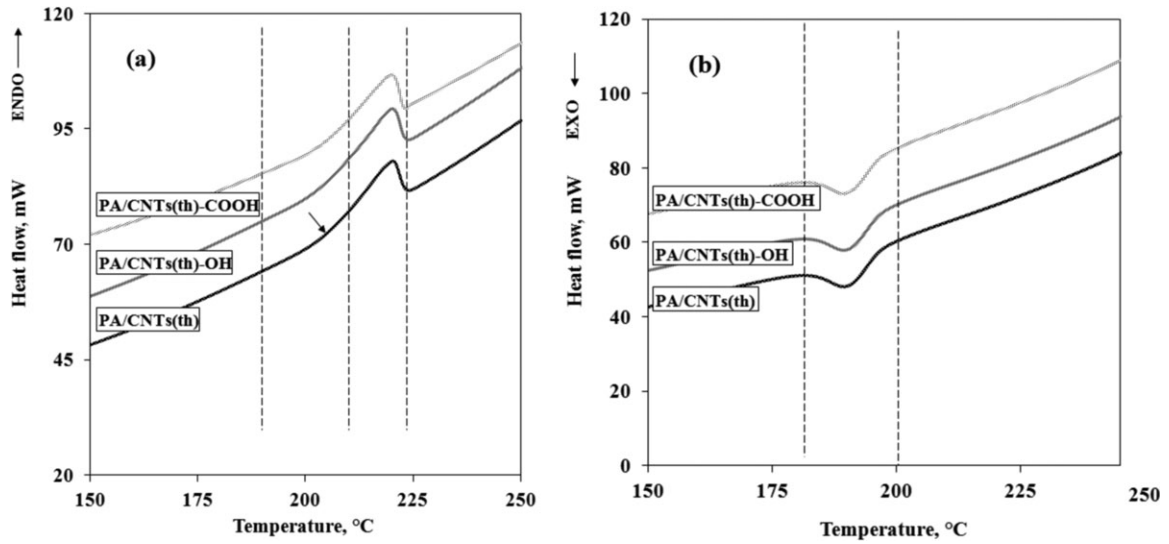


**Figure 12.** DCS traces of the (a) first heating and (b) cooling of CNTs(th) and functionalized CNT(th)-filled PA fibers at the lowest DR (DR = 1).

highest DR for the CNTs(th) and even more for the CNT(uth)-PA-based systems. The intrinsic waviness, the folding tendency, and the functional groups on the CNTs(th) surface hindered the orientation along the flow direction.

## ACKNOWLEDGMENTS

This work was financially supported by the Ministry of University and Research in Italy, FIRB2010 Futuro in Ricerca (project title "GREENER—Toward Multifunctional, Efficient, Safe and Stable 'Green' Bio-Plastics Based Nanocomposites of Technological Interest via the Immobilization of Functionalized Nanoparticles and Stabilizing Molecules;" cod: RBFR10DCS7). Many thanks are due to A. Tito and C. Mazzocchia (Dipartimento di Chimica, Materiali e Ingegneria Chimica "G. Natta," Politecnico di Milano) for supplying the MW-CNTs with ultrathin outer diameters.

## REFERENCES

1. Baughman, R. H.; Zakhidov, A. A.; De Heer, W. A. *Science* **2002**, *297*, 787.
2. Dai, H. *Surf. Sci.* **2002**, *500*, 218.
3. Iijima, S. *Phys. B* **2002**, *323*, 1.
4. Zhang, W. D.; Shen, L.; Phang, I. Y.; Liu, T. *Macromolecules* **2004**, *37*, 256.
5. Xie, X.; Mai, Y.; Zhou, X. *Mater. Sci. Eng. Rep.* **2005**, *49*, 89.
6. Li, Y.; Shimizu, H. *Polymer* **2007**, *48*, 2203.
7. Gojny, F. H.; Wichmann, M. H. G.; Fiedler, B.; Schuilte, K. *Compos. Sci. Technol.* **2005**, *65*, 2300.
8. Morcom, M.; Atkinson, K.; Simon, G. P. *Polymer* **2010**, *51*, 3540.
9. Lopez Gaxiola, D.; Jubinski, M. M.; Keith, J. M.; King, J. A.; Miskioglu, I. J. *Appl. Polym. Sci.* **2010**, *118*, 1620.
10. Lin, Y.; Zhou, B.; Fernando, K. A. S.; Liu, P.; Allard, L. F.; Sun, Y. P. *Macromolecules* **2003**, *36*, 7199.
11. Lin, Y.; Meziani, M. J.; Sun, Y. P. *J. Mater. Chem.* **2007**, *17*, 1143.
12. Hudson, J. L.; Jian, H.; Leonard, A. D.; Stephenson, J. J.; Tour, J. M. *Chem. Mater.* **2006**, *18*, 2766.
13. Tasis, D.; Tagmatarchis, N.; Bianco, A.; Prato, M. *Chem. Rev.* **2006**, *106*, 1105.
14. Ebbesen, T. W.; Ajayan, P. M.; Hiura, H.; Tanigaki, K. *Nature* **1994**, *367*, 519.
15. Georgakilas, V.; Kordatos, K.; Prato, M.; Guldi, D. M.; Holzingger, M.;, Hirsch, A. J. *Am. Chem. Soc.* **2002**, *124*, 760.
16. Chen, R. J.; Zhang, Y.; Wang, D.; Dai, H. J. *Am. Chem. Soc.* **2001**, *123*, 3838.
17. Li, H.; Cheng, F.; Duft, A. M.; Adronov, A. J. *Am. Chem. Soc.* **2005**, *127*, 14518.
18. Beyer, G. Industry Guide to Polymer Nanocomposites; Plastics Information Direct: Bristol, United Kingdom, **2009**.
19. Sennett, M.; Welsh, E.; Wright, J. B.; Li, W. Z.; Wen, J. G.; Ren, Z. F. *Appl. Phys. A* **2003**, *76*, 111.
20. Bhattacharyya, A. R.; Sreelumar, T. V.; Liu, T.; Kumar, S.; Ericson, L. M.; Hauge, R. H.; Smalley, R. E. *Polymer* **2003**, *44*, 2373.
21. Potschke, P.; Brunig, H.; Janke, A.; Fischer, D.; Jehnichen, D. *Polymer* **2005**, *46*, 10355.
22. Sandler, J. K. W.; Pegel, S.; Cadek, M.; Gojny, F.; Es, M.; Lohmar, J.; Blau, W. J.; Schulte, K.; Windle, A. H.; Shaffer, M. S. P. *Polymer* **2004**, *45*, 2001.
23. Dintcheva, N. T.; Arrigo, R.; Nasillo, G.; Caponetti, E.; La Mantia, F. P. *Macromol. Mater. Eng.* **2011**, *296*, 645.
24. Dintcheva, N. T.; Arrigo, R.; Morreale, M.; La Mantia, F. P.; Matassa, R.; Caponetti, E. *Polym. Adv. Technol.* **2011**, *22*, 1612.
25. La Mantia, F. P.; Dintcheva, N. T.; Scaffaro, R.; Marino, R. *Macromol. Mater. Eng.* **2008**, *293*, 83.
26. Konell, J. P.; King, J. A.; Miskioglu, I. J. *Appl. Polym. Sci.* **2003**, *90*, 1716.
27. Halpin, J. C.; Kardos, J. L. *Polym. Eng. Sci.* **1976**, *15*, 344.
28. Thostenson, E. T.; Chou T. W. *J. Phys. D: Appl. Phys.* **2003**, *36*, 573.